MIMO IMPEDANCE MODELLING OF GRID FOLLOWING INVERTER WITH LOCAL VOLTAGE CONTROL

Georgia Saridaki[1], Panos Kotsampopoulos[1], Nikos Hatziargyriou[1], Xi Luo[2], Efstratios Batzelis[2], Abhinav Singh[2]

[1]School of Electrical and Computer Engineering, National Technical University of Athens, Greece
2 School of Electronics and Computer Science, University of Southampton, Southampton, UK

Keywords: GRID-FOLLOWING (GFL) INVERTER, MIMO IMPEDANCE MODELLING, LOCAL VOLTAGE CONTROL, FAST-INTERACTIONS CONVERTER-DRIVEN STABILITY (FICDS), IMPEDANCE BASED ANALYSIS.

Abstract

In recent years, in response to the global climate crisis, inverter-based energy resources (IBRs) have been massively integrated into power systems. Their effective operation and control lie on a wide variety of inner, outer, and synchronization control loops which have been reported to interact and compromise power system's stability. In this study, a Multi-Input-Multi-Output (MIMO) impedance model for a three-phase grid following inverter with local voltage control has been proposed. This linear time invariant model takes into consideration the delay and the coupling between the control blocks and serves as a simpler and more computationally efficient method to capture oscillations and interactions in time and frequency domain. It can predict instabilities caused by the different control layers along with the frequencies of the oscillations. The effect of the delay, the current control tuning parameters and the interactions between the current controller and the local voltage controller have been highlighted. The results have been validated in time and frequency domain simulations in SIMULINK environment.

1. Introduction

The transformation of the energy sector and the massive integration of renewable energy has led to the wide uptake of inverter-based resources (IBRs) posing significant challenges regarding power system stability and reliability. By integrating control schemes, such as outer droop controls for absorbing/injecting active/reactive power in grid-following (GFL) mode or directly controlling the voltage in grid-forming (GFM) mode, IBRs can effectively provide support in the traditional power system stability categories (voltage, frequency, and rotor angle stability).

However, these control schemes together with the inner inverter control loops, operate in a wide frequency range and have been reported to interact and raise converter-driven instabilities [1]. Several studies have shed light on the mechanisms that affect this type of stability. For example, oscillations in high frequencies (typically 100 Hz -10 kHz) have been caused by control delays (such as telecommunication and PWM delay) [2]. The inner loop controls of inverters have also been reported to interact with other inverters connected to close proximity and with passive elements of the grid [3] [4]. For this type of stability, which is classified as Fast-Interactions Converter-driven stability (FICDS) [1], several control system criteria have been proposed that are applicable to inverters connected to the same node such as the minor loop gain (MLG), global minor loop gain (GMLG) and the global admittance (GA) criterion which evaluate the system stability by plotting the Nyquist diagram of MLG, GMLG transfer functions and tracking the poles of the GA admittance respectively [5] [6] [7]. Instabilities in low frequencies have been linked to the Phase-locked-loop (PLL), which is crucial for the synchronization of the inverter with the grid, the interactions between outer droop controls and the grid strength [8]. Although, there have been extensive efforts from both industry and academia, these observations have been mainly based on theoretical analysis and modelling of a fixed power system topology, which has been verified with simulations and real time experiments; a concrete unified mathematical methodology for assessing converter driven stability that can be adapted to larger systems with multiple inverters is still missing. Some efforts in the inverter MIMO design can be found in literature but don't take into consideration the coupling of the d-q axes in the current control and the outer control loops [9], [10].

In this study, a linear MIMO impedance model for GFL inverter with local voltage controller has been designed in the frequency frame taking into consideration the coupling between the d-q axes of the current controller and the coupling between the current and voltage control loops. The stability of this MIMO model is assessed for different parameters by tracking its poles' location which is a simple approach that doesn't require extensive algorithmic complexity and can be expanded to larger scale networks. With this model, the effect of the tuning parameters, the delay, and the local voltage controller along with the correlation between these parameters of interest is investigated. In the unstable cases, the frequencies of oscillations are calculated and are compared with time domain simulations with the use of SIMULINK environment.

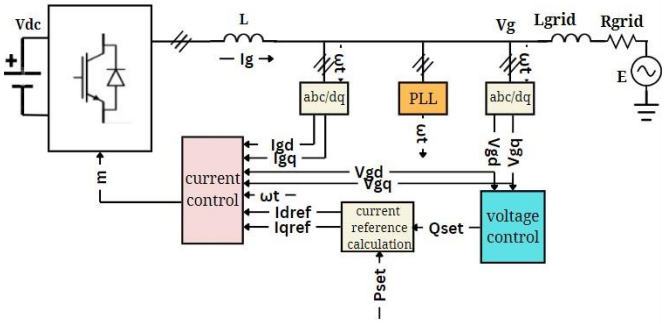

Fig. 1 Three phase GFL inverter with local voltage control.

2. Methodology

For the evaluation of FICDS, the impedance-based stability analysis has been applied which requires modelling of each component as a linear time invariant transfer function in the frequency domain [11]. Then, the stability of the power system can be evaluated by applying classical control systems theory to the matrix of the system. Some of the significant advantages of this method are that it requires less computational effort than the state-space analysis and is easily applicable to larger power systems [12].

2.1. Linear modelling of inverter blocks

A typical topology for a three-phase GFL inverter with local voltage control has been designed and is illustrated in Fig.1 Linear models for the control blocks of the voltage droop, the current reference regulation, the current control, the filter, and the grid have been adapted and are illustrated in Fig. 2, 3, and 4 respectively as explained below in 2.1.1. and 2.1.2.

2.1.1 Local voltage control: The voltage control consists of a Q-V droop characteristic which calculates the setpoint of the reactive power Q_{set} based on the measured value of $\bar{V} = \sqrt{{V_{gd}}^2 + {V_{gq}}^2}$, where V_{gd}, V_{gq} variables correspond to the d-q components of the voltage at the point of connection, and the nominal voltage V_{nom} [13]. The droop gain is calculated as m=DQ/DV, whereas DQ is the deviation of reactive power (per unit) and DV is the deviation of voltage (per unit). The current reference calculation takes as inputs the set points for active and reactive power and produces the reference output currents for the inverter I_{dref}, I_{qref}. Assuming that the q component of V_g is set to zero (i.e. PLL robustly locked onto the PCC voltage), the block diagram of Fig. 2 can be produced. In order to extract the transfer functions I_{qref}/V_{nom}, I_{qref}/V_{gd} and I_{dref}/P_{set} which incorporate non-linear elements, the linearization tool of MATLAB has been used.

$$(V_{nom} - V_{gd}) * m * Q_{max} = Q_{set} \quad (1)$$

$$I_{qref} = \frac{-3}{2 * V_{gd}} * Q_{set} \quad (2)$$

$$I_{dref} = \frac{3}{2 * V_{gd}} * P_{set} \quad (3)$$

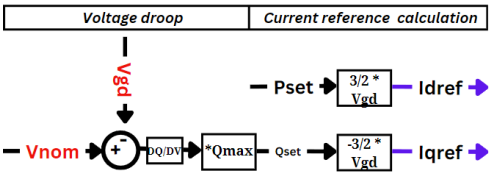

Fig. 2 Block diagram of local voltage control and current reference calculation.

2.1.2 Current control, filter and grid dynamics: The current control, designed in the dq frame, is implemented with a PI controller while the feedforward technique is also applied. The transfer function of the PI controller is $G_{pi}=k_p + k_i/s$. The delay is integrated in the block diagram as second order PADE approximation of $e^{-delay*s}$ function. An L filter in the output of the inverter is used for harmonic mitigation. The U_{cd}, U_{cq}, I_{gd}, I_{gq}, E_d, E_q variables correspond to the d-q components of the inverter output voltage, the inverter output current and the voltage of the grid, respectively. Using the equations (4), (5) and (6), (7), the linear block diagrams of Fig. 3 and Fig. 4 representing the current control and the filter and grid dynamics, respectively, have been produced.

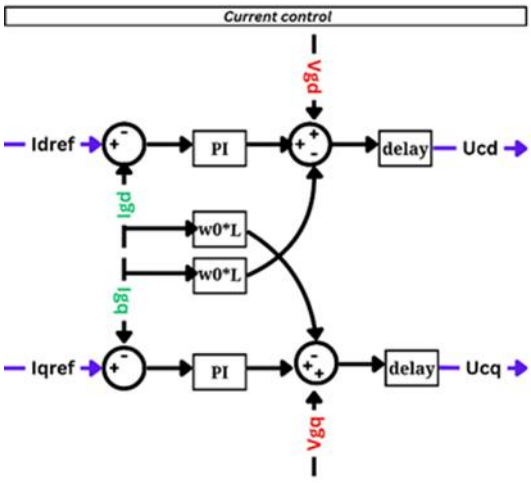

Fig. 3 Block diagram of Current control

$$\left[(I_{dref} - I_{gd}) * G_{pi} + U_{gd} - I_{gq} * L * \omega_0\right] * delay = U_{cd} \quad (4)$$

$$\left[(I_{qref} - I_{gq}) * G_{pi} + U_{gq} - I_{gd} * L * \omega_0\right] * delay = U_{cq} \quad (5)$$

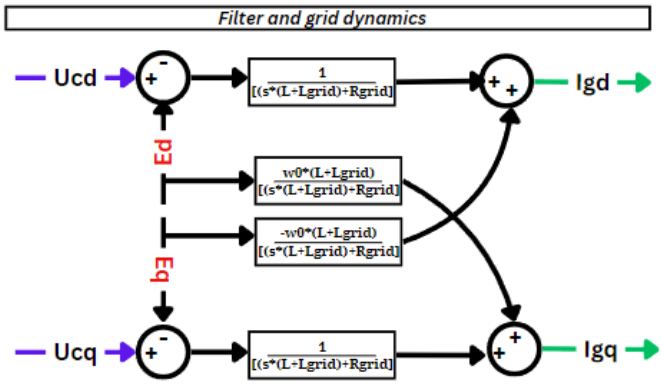

Fig. 4 Block diagram of filter and grid dynamics

$$I_{gd} = \frac{\omega_0 * (L + L_{grid})}{s * (L + L_{grid}) + R_{grid}} * I_{gq} + \frac{U_{cd} - E_d}{s * (L + L_{grid}) + R_{grid}} \quad (6)$$

$$I_{gq} = \frac{-\omega_0 * (L + L_{grid})}{s * (L + L_{grid}) + R_{grid}} * I_{gd} + \frac{U_{cd} - E_d}{s * (L + L_{grid}) + R_{grid}} \quad (7)$$

2.2. *MIMO model*

By using the system's equations (1) – (7) for each control block, a MIMO model is produced with inputs the reference active power of the inverter P_{set}, V_{nom}, V_{gd}, V_{gq}, E_d , E_q. The output of the model is the d-q components of the I_g output current, i.e. GFL is modelled as a voltage-dependent current source. It is worth noting that the coupling between the d-q axes and the different control blocks (e.g. between the current controller and the local voltage control) has been taken into consideration. The stability of the MIMO model is assessed by tracking the location of the [C] matrix poles, which incorporates the dynamics of the control blocks, the delay, the filter and the grid dynamics.

$$\begin{bmatrix} I_{gd} \\ I_{gq} \end{bmatrix} = [\boldsymbol{C}] * \begin{bmatrix} P_{set} \\ V_{nom} \\ V_{gd} \\ V_{gq} \\ E_d \\ E_q \end{bmatrix}$$

$$[\boldsymbol{C}] = \begin{bmatrix} \frac{-E\Gamma}{\Gamma^2 + \Delta^2} & \frac{H\Gamma}{\Gamma^2 + \Delta^2} & \frac{delay - BZ}{2B\Gamma} & \frac{\Gamma delay}{B(\Gamma^2 + \Delta^2)} & \frac{-\Gamma}{B(\Gamma^2 + \Delta^2)} & \frac{-\Gamma}{B(\Gamma^2 + \Delta^2)} \\ \frac{-E\Delta}{\Gamma^2 + \Delta^2} & \frac{-H\Delta}{\Gamma^2 + \Delta^2} & \frac{delayBZ - 2BZ}{2B\Gamma} & \frac{-\Delta delay}{B(\Gamma^2 + \Delta^2)} & \frac{-\Delta}{B(\Gamma^2 + \Delta^2)}) & \frac{-\Delta}{B(\Gamma^2 + \Delta^2)} \end{bmatrix}$$

where:

$\boldsymbol{\Gamma} = 1 + \frac{G_{pi} delay}{B}$, $\boldsymbol{\Delta} = -A + \frac{L\omega_0 delay}{B}$, $\boldsymbol{E} = G_{pi} delay * I_{dref}/P_{set}$, $\boldsymbol{Z}$=I_{qref}/V_{gd} , $\boldsymbol{H}$=I_{qref}/V_{nom}

$\boldsymbol{A} = \frac{\omega_0 * (L + L_{grid})}{s * (L + L_{grid}) + R_{grid}}$, $\boldsymbol{B}$= $s * (L + L_{grid}) + R_{grid}$

3. Results

3.1. *MIMO model*

The [C] matrix has been produced in MATLAB for the system of Fig.1 with the parameters of Table 1.

Table 1 System parameters

Current controller (PI)	K_{p1}=3000, K_{i1}=3000
Droop control	m=-33 (DV=3%, DQ= -1)
L Filter	0.03pu
Grid	0.3 Ω/0.1mH
delay	0.2ms
Base voltage	400V
Base power	10kW
System frequency	50Hz

3.1.1 Impact of current control tuning parameters: The current controllers of the inverters have been reported to compromise systems stability if they are not tuned correctly in several case scenarios [3]. For investigating the impact of the PI tuning parameters to the MIMO's stability, a parametric analysis for different values of the PI's proportional and integral gain has been conducted by tracking the MIMO poles location. It can be seen in Table 2 that when k_p and k_i exceed the value of 3800, the MIMO model demonstrates poles in the right half plane. When k_p and k_i further increase to 4200, there are two pairs of eigenvalues dominating the instability at frequencies of 7824 Hz and 8284 Hz. Then, by varying the different controller gains, the oscillation frequencies of the instability are extracted from the MIMO model, as shown in Figure 5. These frequencies start from 7,834kHz to 8,645kHz matching well with several published works that have reported that the current controllers can lead to FICDS instability phenomena in high frequencies (100- 10kHz).

Table 2 MIMO poles location for different PI tuning parameters

Proportional gain of PI controller (k_p)	Internal gain of PI controller (k_i)	MIMO poles in the right half plane
3000	3000	none
3200	3200	none
3400	3400	none
3600	3600	none
3800	3800	8 ±1300i
4000	4000	146±7642i
4200	4200	165±7824i, 273±8284i

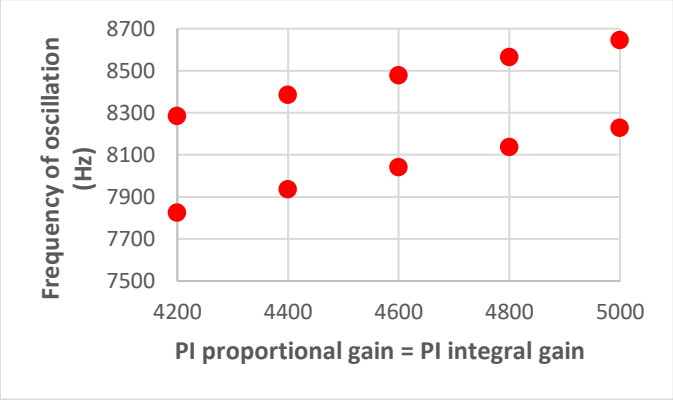

Fig. 5 Frequencies of oscillation for different k_p (k_i = k_p for all cases) extracted from MIMO model.

3.1.2 Impact of delay: Several different categories of delays can be found in real power systems introduced by the PWM technique, the telecommunications delay e.g. between inverters and central controllers, the voltage RMS computation and the filters to smoothen the voltage. These delays should not be neglected as they seem to drastically affect the stability of the system [13].

The impact of the delay has been investigated by calculating the MIMO poles in the right half plane starting from 0.1ms

delay to 0.35ms. According to the results of Table 3, from 0.1ms to 0.25ms the system is stable and when it exceeds the value of 0.3ms two pairs of poles appear in the right half plane.

Table 3 MIMO poles location for different delays

Delay (ms)	MIMO poles in the right half plane
0.1	none
0.15	none
0.2	none
0.25	none
0.3	375 ± 5696i
	258 ± 5254i
0.35	667 ±5084i
	533 ± 4678i

Moreover, to investigate the interaction between the delay and the current controller a parametric analysis with different k_p (equal to k_i) for different values of the delay has been conducted by plotting the poles of the MIMO model. The results are presented in Fig. 6, where the green dots correspond to stable cases and the red dots correspond to unstable cases. The green curve corresponds to the stability boundary with regard to these two parameters, for the system under test.

For delay corresponding to 0.1ms the system becomes unstable when the proportional and integral gain are set to 8000. The increase of delay from 0.1ms to 0.15ms affects the boundary of the PI controller which moves to 6000. The further increase of the delay leads to the decrease of the PI tuning boundary: for delay of 0.25ms the MIMO is stable only if the proportional and internal gain are set to 3000 and is unstable for all the other cases. Through this analysis it is revealed that there is a correlation between these two factors which can be used to improve the performance of the power systems.

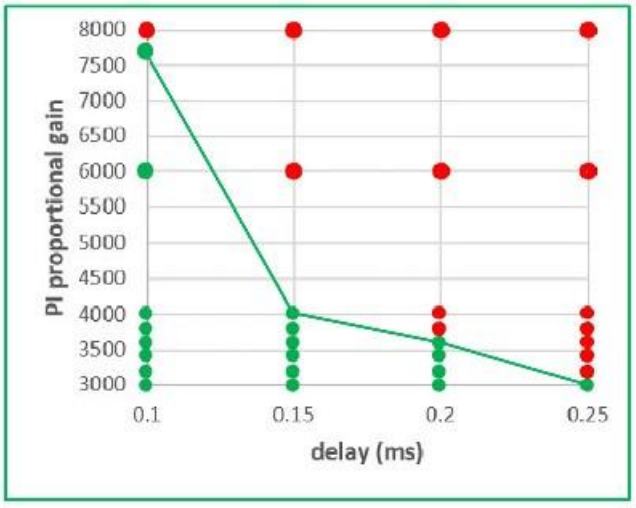

Fig.

6 Effect of the delay to the PI tuning boundary and stability boundary.

3.1.3 Impact of local voltage controller: Grid following inverters providing ancillary services to the grid have become an active topic of discussion and gained increased interest in recent years [14]. A common approach is the implementation of a local voltage controller with a droop characteristic that enables the inverter to inject or absorb reactive power if there is voltage drop or rise.

To investigate the interaction of this control block with the current controller, the poles of the MIMO model have been calculated and are presented in Table 4. It can be seen that for k_p=3800, k_i=3800 the MIMO is stable if the reactive power set point is constant, but it demonstrates a set of poles in the right half plane when the local voltage control is activated. This instability can be potentially linked to the additional loop of V_{gd} that is introduced in the system (Fig. 2).

Moreover, the effect of the change of the droop gain is illustrated in Table 5. For a stable case with k_p=3300, k_i=3300 and droop gain m=-33 when the droop gain changes to -100, the MIMO demonstrates one set of poles in the right half plane leading to the conclusion that a steep slope can potentially lead to converter driven instability if the PI controller is not tuned correctly.

Table 4 MIMO poles location without and with local voltage controller (k_p=3800, k_i=3800)

Local voltage controller	MIMO poles in the right half plane
no	none
yes (m=-33)	8 ±1300i

Table 5 MIMO poles location with different voltage droop gain (k_p=3300, k_i=3300)

m	MIMO poles in the right half plane
3% (m=-100)	none
1% (m=-33)	313 ± 7670i

3.2. Simulink validation

For the validation of the theoretical results obtained from the MIMO model, a time domain simulation for the non-linear system of Fig. 1 has been designed in SIMULINK/SimPowerSystems. Moreover, the Model linearizer tool has been used to extract the frequency of the oscillations.

Firstly, it can be seen in Fig. 7 (a) that when the current controller parameters change from k_{p1}=3000, k_{i1}=3000 to k_{p2}=4000, k_{i2}=4000 at t=0.2s, the output current of the inverter is unstable with one set of poles at 129±7818i matching well with the results obtained from the MIMO model in Table 2. At t=0.22s the delay is decreased from 0.2ms to 0.1ms (Fig. 7 (b)) and the system becomes stable again, as expected from the MIMO analysis of Fig. 6. Then, for an increase of the delay from 0.2ms to 0.3ms (k_{p1}=3000 k_{i1}=3000) the system demonstrates two set of poles at 394±5350i and 239±5600i, which are reasonably close to the results of Table 3.

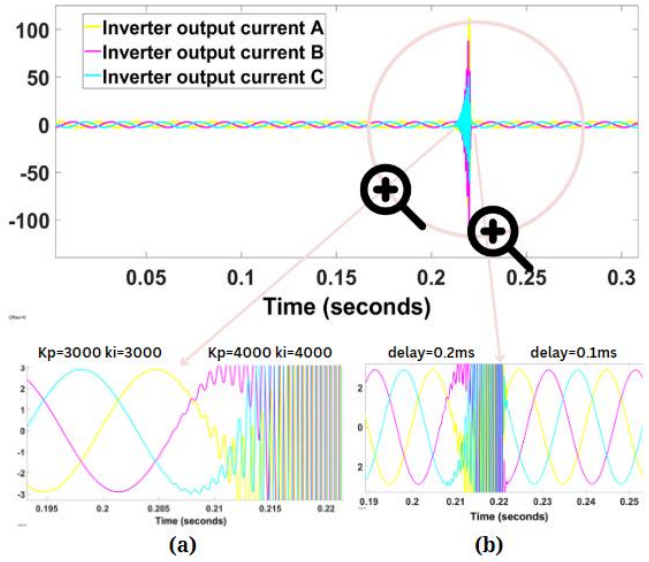

Fig. 7 Output current of the inverter (a) at t=0.2s PI tuning parameters increase, (b) at t=0.22s, the delay is decreased.

Additionally, for the same range of k_p illustrated in Fig. 5, the frequencies of oscillations have been measured in the time domain simulations and are illustrated in Fig. 8 with orange dots while the red dots correspond to the unstable measured frequencies extracted from the MIMO model. Fig. 8 shows that the MIMO model matches well with the SIMULINK results. It can be seen that there is a small deviation between the results of the two figures, which is expected due to the assumptions that have been made in the linear modelling of MIMO components and are not incorporated in the full non-linear time simulation. Nevertheless, the MIMO model can detect the unstable cases and the frequencies of the oscillation with an acceptable accuracy.

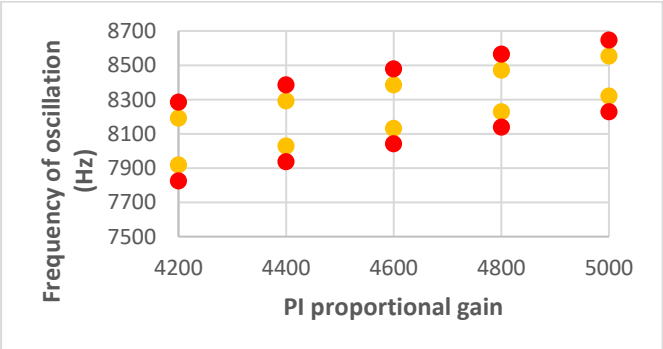

Fig. 8 Frequencies of oscillation for different PI tuning parameters (red dots correspond to the MIMO results and orange dots correspond to the SIMULINK results).

Lastly, in Fig. 9 (a) it can be seen that for current control parameters of k_{p3}=3300 and k_{i3}=3300 the system remains stable after the activation of the local voltage control at t=0.5s. For k_{p4}=3800 and k_{i4}=3800, the system becomes unstable when the same voltage droop characteristic is implemented, which matches well with the results in Table 4 (Fig. 9 (b)). For an inverter with k_{p3}=3300 and k_{i3}=3300, a pole zero map has been plotted in the SIMULINK environment (Fig. 10) which reveals that for a change of voltage droop gain from m=-33 to m=-100, the critical pole moves from the left half plane to the right half plane, indicating that the system demonstrates unstable behaviour, matching well with the MIMO results of Table 5.

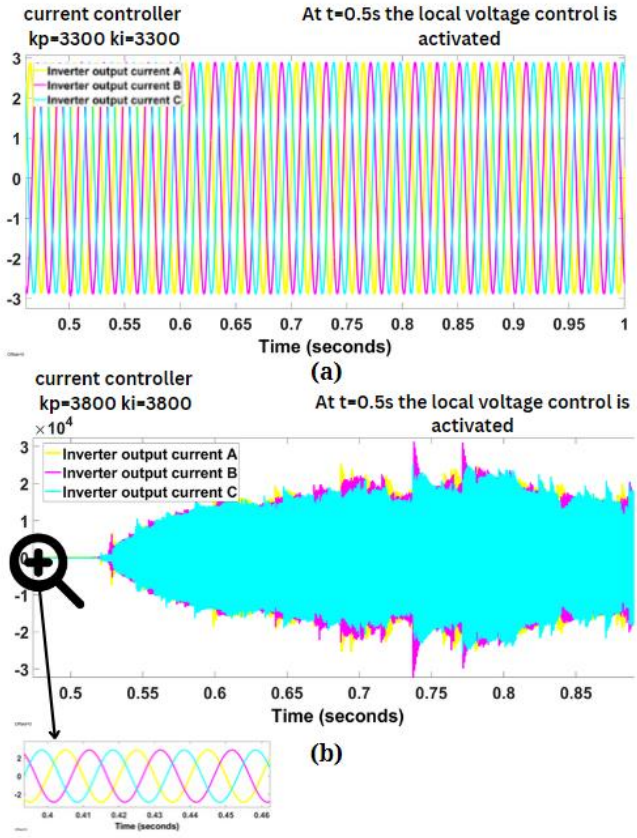

Fig. 9 Output current of the inverter (a) K_{p1}=3000 K_{i1}=3000 and at t=0.5s the local voltage controller is activated, (b) K_{p2}=3800 K_{i2}=3800 and at t=0.5s the local voltage controller is activated.

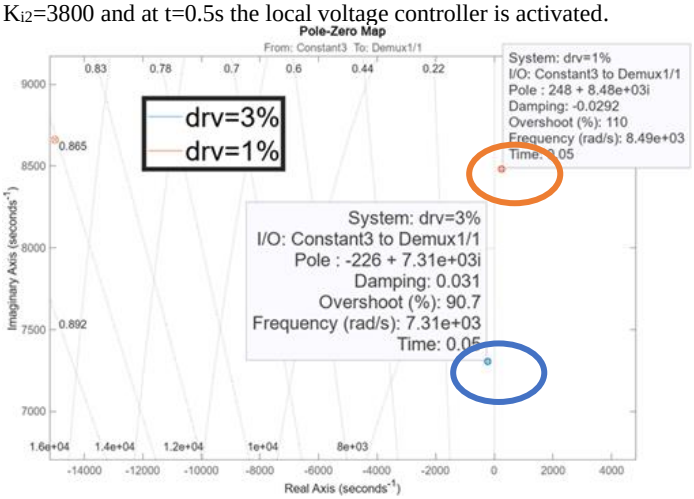

Fig. 10 System's poles location when voltage droop gain changes from -33(DV=3%, DQ=-1) to -100 (DV=1%, DQ=-1).

4. Conclusion

This paper introduces a simple MIMO model in the frequency frame that tracks the Fast-Interaction Converter-driven

(FICDS) instability phenomena and the corresponding frequencies of oscillation effectively with the use of the impedance-based analysis. The MIMO results are validated with time domain simulations from which the oscillatory frequencies are extracted.

Firstly, it is observed that the increase of the current tuning parameters and the increase of the delay can raise instabilities to the system, while the increase of the delay leads to the decrease of the stability boundary of the current tuning parameters. Moreover, the additional loop of the voltage droop can cause instability if the current controllers are not tuned correctly. Lastly, the increase of the droop gain for fixed current tuning parameters can potentially interact with the current controllers and compromise the stability of the system. Regarding future work, a MIMO model for Grid-forming (GFM) inverter can provide further insight into the interactions of GFL-GFM inverters which is a very active topic of research in recent years. By adding multiple inverters, the applicability of the model to larger power networks with less computational effort will be highlighted.

5. Acknowledgements

This work has been conducted within UNIFORM project and supported by UKRI under Grant agreement EP/Y001575/1 and ROSES project (EP/T021713/1). It was also financially supported by the European Union's Horizon 2020 Research and Innovation Program and the Department of Science and Technology (DST), India through the RE-EMPOWERED Project under Grant Agreement No 101018420 and DST/TMD/INDIA/EU/ILES/2020/50(c) respectively.

6. References

[1] N. Hatziargyriou et al, “Stability definitions and characterization of dynamic behavior in systems with high penetration of power electronic interfaced technologies.” IEEE PES-TR77

[2] L. Kong, Y. Xue, L. Qiao and F. Wang, "Review of Small-Signal Converter-Driven Stability Issues in Power Systems," in IEEE Open Access Journal of Power and Energy, vol. 9, pp. 29-41, 2022,

[3] X. Wang, F. Blaabjerg, and W. Wu, “Modeling and analysis of harmonic stability in an AC power-electronics-based power system,” IEEE Trans. Power Electron., vol. 29, no. 12, pp. 6421–6432, 2014, doi: 10.1109/TPEL.2014.2306432.

[4] G. Saridaki, A. G. Paspatis, P. Kotsampoupoulos and N. Hatziargyriou, “An investigation of factors affecting Fast-Interaction Converter-driven stability in Microgrids” in Electric Power Systems Research,Volume 223, 2023, 109610

[5] J. Sun, “Impedance-based stability criterion for grid-connected inverters,” IEEE Trans. Power Electron., vol. 26, no. 11, pp. 3075–3078, 2011, doi: 10.1109/TPEL.2011.2136439.

[6] Q. Ye, R. Mo, Y. Shi, and H. Li, “A unified Impedance-based Stability Criterion (UIBSC) for paralleled grid-tied inverters using global minor loop gain (GMLG),” in 2015 IEEE Energy Conversion Congress and Exposition, ECCE 2015, Oct. 2015, pp. 5816–5821, doi: 10.1109/ECCE.2015.7310476.

[7] W. Cao, S. Wang, H. Kang, K. Liu, Q. Wang and J. Zhao, "Inherent Interaction Analysis for Harmonic Oscillations in the Multi-Paralleled Grid-Connected Inverter System Using a Sum Type Criterion: Global Admittance (GA)," in IEEE Access, vol. 8, pp. 8275-8285, 2020

[8] Z. Zou et al., "Modeling and Control of a Two-Bus System With Grid-Forming and Grid-Following Converters," in IEEE Journal of Emerging and Selected Topics in Power Electronics, vol. 10, no. 6, pp. 7133-7149, Dec. 2022.

[9] Ye Zhang, Muqin Tian, Hong Zhang, Jiancheng Song, Wenjie Zhang, ‘’Admittance Modeling and Stability Enhancement of Grid-connected Inverter Considering Frequency Coupling in Weak Grids’’, Electric Power Systems Research, Volume 209, 2022, 108034, ISSN 0378-7796

[10] X. Wang, L. Harnefors and F. Blaabjerg, "Unified Impedance Model of Grid-Connected Voltage-Source Converters," in IEEE Transactions on Power Electronics, vol. 33, no. 2, pp. 1775-1787, Feb. 2018

[11] S. Song, Z. Wei, Y. Lin, B. Liu and H. Liu, "Impedance modeling and stability analysis of PV grid-connected inverter systems considering frequency coupling," in CSEE Journal of Power and Energy Systems, vol. 6, no. 2, pp. 279-290, June 2020

[12] H. Wu, F. Zhao and X. Wang, "A Survey on Impedance-Based Dynamics Analysis Method for Inverter-Based Resources," in IEEE Power Electronics Magazine, vol. 10, no. 3, pp. 43-51, Sept. 2023

[13] F. Andrén, B. Bletterie, S. Kadam, P. Kotsampopoulos and C. Bucher, "On the Stability of Local Voltage Control in Distribution Networks With a High Penetration of Inverter-Based Generation," in IEEE Transactions on Industrial Electronics, vol. 62, no. 4, pp. 2519-2529, April 2015

[14] Lucas S. Xavier, Allan F. Cupertino, Heverton A. Pereira, Ancillary services provided by photovoltaic inverters: Single and three phase control strategies, Computers & Electrical Engineering, Volume 70, 2018